

SlimEdge: Lightweight Distributed DNN Deployment on Constrained Hardware

Mahadev Sunil Kumar^{a,*}, Arnab Raha^b, Debayan Das^c, G. Gopakumar^d,
Amitava Mukherjee^e

^a*Accenture PLC, Bengaluru, Karnataka, India*

^b*Intel Corporation, California, United States of America*

^c*Indian Institute of Science, Bengaluru, Karnataka, India*

^d*Amrita Vishwa Vidyapeetham, Kollam, Kerala, India*

^e*Birla Institute of Technology and Science, Dubai, United Arab Emirates*

Abstract

Deep distributed networks (DNNs) have become central to modern computer vision, yet their deployment on resource-constrained edge devices remains hindered by substantial parameter counts and computational demands. Here, we present an approach to the efficient deployment of distributed DNNs that jointly respects hardware limitations and preserves task performance. Our method integrates a structured model pruning with a multi-objective optimization to tailor network capacity to heterogeneous device constraints. We demonstrate this framework using Multi-View Convolutional Neural Network (MVCNN), a state-of-the-art architecture for 3D object recognition, by quantifying the contribution of individual views to classification accuracy and allocating pruning budgets, respectively. Experimental results show that the resulting models satisfy user-specified bounds on accuracy and memory footprint while reducing inference latency by factors ranging from 1.2x to 5.0x across diverse hardware platforms. These findings suggest that performance-aware, view-adaptive compression provides a viable pathway for deploying complex vision models in distributed edge environments.

Keywords:

Neural Networks, Convolutional Neural Networks, Edge Computing,
Distributed Inference, Optimization,

1. Introduction

The deployment of DNNs on resource-constrained edge devices has become a major challenge in the widespread availability of Internet of Things (IoT) ecosystems. While modern architectures achieve high accuracy in tasks such as 3D object recognition, their computational and memory requirements often exceed the capabilities of low-power hardware commonly found in edge devices. This problem raises a fundamental question: how can complex vision models be adapted to heterogeneous edge devices without compromising task performance?

Multi-View inference offers a natural setting in which this problem manifests. In systems such as the Multi-View Convolutional Neural Network (MVCNN) Su et al. (2015), a state-of-the-art architecture for 3D object recognition, where distinct 2D images of an object are processed in parallel by separate feature extractors. These are typically deployed across multiple edge nodes, before feature aggregation, and classification at a central server. As illustrated in Figure 1, such a configuration might involve a roadside monitoring system, where each camera feeds into a local edge device tasked with extracting view-specific features for classifying vehicles such as cars and trucks to calculate traffic violations and road traffic conditions. Using multiple perspectives of 3D objects has shown greater accuracy and performance when compared to using just one view as illustrated by Su et al. (2015). But, while this distributed design enables spatial parallelism, it also exposes the system to the combined constraints of per-device memory budgets, variable compute capacities, and global accuracy requirements.

Standard models, often trained without hardware awareness, exceed the memory or latency limits of typical edge devices like Raspberry Pi or Nvidia Jetson Nano devices. Moreover, uniform model compression, such as applying identical pruning ratios across all views, fails to account for two critical asymmetries: (i) the unequal contribution of individual views to classification accuracy, and (ii) the heterogeneous computational capabilities of the devices hosting them.

*Corresponding author

Email addresses: mahadevsunilkumar03@gmail.com (Mahadev Sunil Kumar),
arnab.raha@intel.com (Arnab Raha), debayanandas@iisc.ac.in (Debayan Das),
gopakumarg@am.amrita.edu (G. Gopakumar), amitava@dubai.bits-pilani.ac.in
(Amitava Mukherjee)

URL: <https://mahadevsunilkumar.com> (Mahadev Sunil Kumar),
<https://arnabraha.net> (Arnab Raha),
<https://eecs.iisc.ac.in/people/debayan-das/> (Debayan Das),
<https://www.amrita.edu/faculty/gopakumarg/> (G. Gopakumar),
<https://www.bits-pilani.ac.in/dubai/dr-amitava-mukherjee/> (Amitava Mukherjee)

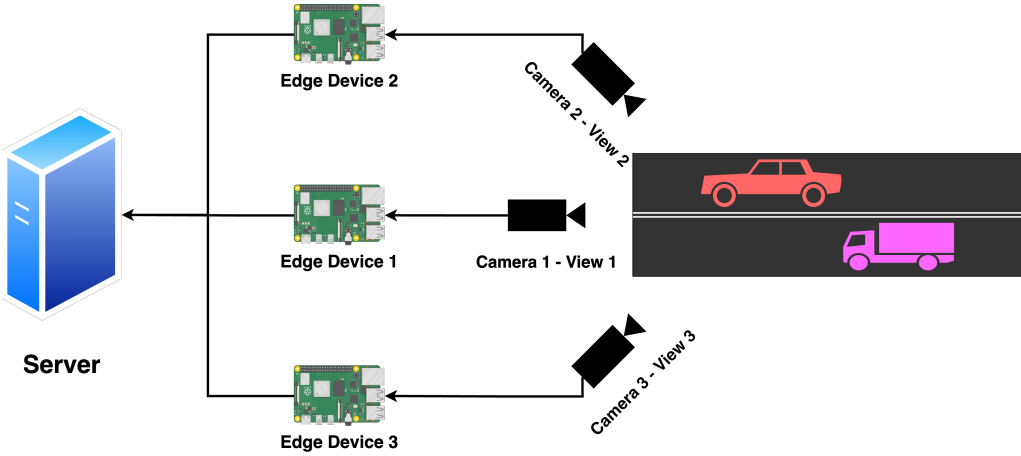


Figure 1: Roadside Vehicle Monitoring System using 3 Cameras

Aggressive pruning of highly informative views on capable hardware, or insufficient compression on weak devices, can degrade the accuracy or violate memory constraints, respectively.

To address these issues, we introduce SlimEdge, a framework for view and device-aware model compression. Our approach begins by quantifying the importance of each view, as well as the per-view device metrics to guide a pruning process that respects user defined constraints on accuracy and model size. The SlimEdge then generates a set of models, each tailored to its host device while collectively satisfying global performance targets.

The main contributions of this paper are:

1. **Metric Formulation:** We propose an objective function that simultaneously quantifies view-importance via Taylor expansion and device capability via normalized latency.
2. **Optimization Strategy:** We introduce a biased-initialization NSGA-II approach that utilizes Beta-distribution sampling to accelerate convergence in high-dimensional pruning spaces.
3. **Real-World Validation:** We deploy the framework on a physical cluster of heterogeneous Raspberry Pi devices, demonstrating a 3.94x latency reduction compared to uniform pruning baselines.

This work transcends static, one-size-fits-all compression, adopting a dynamic deployment strategy. It considers the diverse computing and memory capabilities of each device by compressing each model individually based on the device's specifications. Consequently, the resulting models not only adhere

to stringent memory constraints but also significantly reduce end-to-end latency by factors ranging from 1.2x to 5.0x across heterogeneous platforms. Moreover, these models maintain classification accuracy above user-defined thresholds.

2. Related Work

The deployment of DNNs on resource-constrained edge hardware has become a pivotal challenge at the intersection of machine learning and embedded systems. While contemporary architectures excel in vision tasks, their computational and memory requirements frequently surpass the capabilities of low-power platforms like microcontrollers or single-board computers. This disparity has spurred research on model compression, encompassing techniques such as quantization, coding, and pruning. These methods aim to reduce the parameter count and arithmetic complexity of models while striving to maintain their representational capacity Liang et al. (2021).

Among these approaches, pruning has garnered particular attention due to its compatibility with existing hardware and software stacks. Early pruning methods involved removing individual weights, while more recent techniques operate at a structural level, eliminating entire neurons, channels, or filters Molchanov et al. (2017). Filter pruning presents a favorable trade-off by removing convolutional kernels deemed least important to the loss function. This approach reduces both memory usage and floating-point operations without the need for specialized inference engines. However, most pruning strategies assume a homogeneous deployment target and apply uniform compression across all layers, overlooking the inherent heterogeneity present in distributed edge environments. In parallel, efforts to distribute DNN inference across multiple devices have explored layer-wise partitioning Zhao et al. (2018) or input-dependent offloading Chen et al. (2018). These methods enhance latency by leveraging cloud-edge collaboration, but they often treat the model as a monolithic entity and fail to consider the physical constraints of each node when designing compression. This limitation is particularly evident in multi-view settings, where distinct input streams, such as multiple camera angles of a 3D object, are processed independently before feature aggregation. The MVCNN architecture Su et al. (2015), shown in Figure 1, exemplifies this paradigm, achieving state-of-the-art performance in 3D shape recognition by fusing features from multiple 2D projections. Subsequent refinements, including Latent-MVCNN Yu et al. (2020) and accuracy-optimized variants Angrish et al. (2021), have further demonstrated the effectiveness of view-based fusion. However, none of these works address how to adapt the per-view feature extractors to heterogeneous edge devices with varying

memory budgets and compute capabilities. Existing approaches have a significant limitation: they separate structural importance from deployment context. This means that the contribution of each view to final classification accuracy is not consistent Su et al. (2015). As a result, pruning is applied uniformly across all views. Similarly, device capabilities vary greatly, from Raspberry Pi-class systems to Jetson-class accelerators, but compression is rarely tailored to the specific performance of each device. While recent work has explored hardware-aware neural architecture Baker et al. (2017), these methods are computationally expensive and difficult to integrate into pre-trained models. Others have tried coarse-grained pruning on FPGA-based platforms Yao et al. (2019), but these approaches lack the fine-grained adaptability needed for software-defined edge deployments. The absence of a dynamic framework that considers the memory and computational constraints of edge devices in a distributed system necessitates the development of SlimEdge. This framework addresses three key aspects: (i) the informational asymmetry between different views, (ii) the computational and memory limitations of edge hardware, and (iii) user-defined constraints on the accuracy and size of compressed models. By integrating these dimensions, SlimEdge enables compression to transcend the static one-size-fits-all model and adopt a dynamic, device-sensitive deployment strategy.

3. Methodology

SlimEdge addresses the deployment of MVCNNs across heterogeneous edge devices under hard constraints on model size, accuracy, and inference latency. The algorithm is orchestrated by a central server (Figure 2). It integrates structured pruning, view importance quantification, and multi-objective optimization within a unified pipeline, as detailed in Figure 4. The server generates an optimized model tailored for each edge node, which is subsequently deployed for inference. The central server optimizes the models so that the resultant configuration meets user requirements of the desired accuracy as well as fits within the memory constraints of each of the edge devices.

3.1. ModelNet40 Dataset

The ModelNet40 dataset Wu et al. (2015) serves as a standard benchmark for 3D object recognition, comprising 12,311 CAD models categorized into 40 semantic classes. This dataset allows the use of 3D objects to generate 2D views, which can then be utilized to simulate a distributed environment with multiple edge devices capturing diverse perspectives. Out of the 12,311 CAD models,

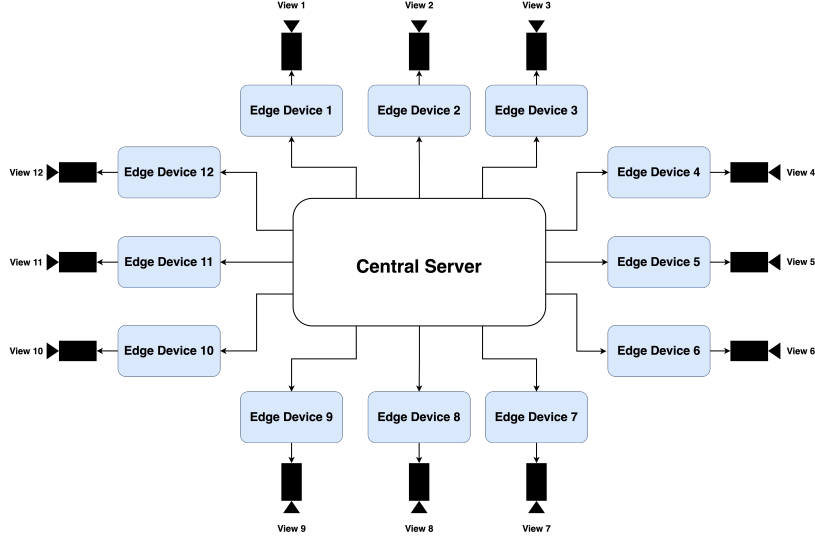


Figure 2: Optimization Framework using 12 Edge Devices

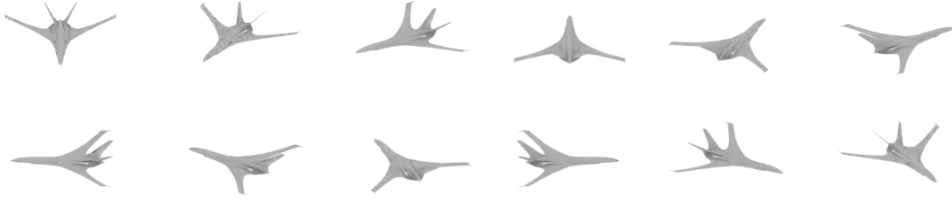


Figure 3: Views of airplane_0006 from 12 different views from the ModelNet40 dataset

9,843 are designated for training, while 2,468 are reserved for testing. To replicate real-world multi-view sensing, each 3D object is rendered from 12 virtual camera positions, uniformly spaced at 30° azimuthal intervals and fixed at a 30° elevation angle Su et al. (2015). Figure 3 illustrates the 12 views when the 3D object "airplane_0006" is employed. This results in a consistent set of 12 two-dimensional projections for each object, which serve as inputs to the distributed feature extractors. The 12 distinct views depicted in Figure 3 enable the model to learn effectively, ultimately leading to improved classification performance.

3.2. *SlimEdge* Architecture

We adopt the Multi-View Convolutional Neural Network Su et al. (2015) paradigm, adapting it for distributed edge deployment. The architecture com-

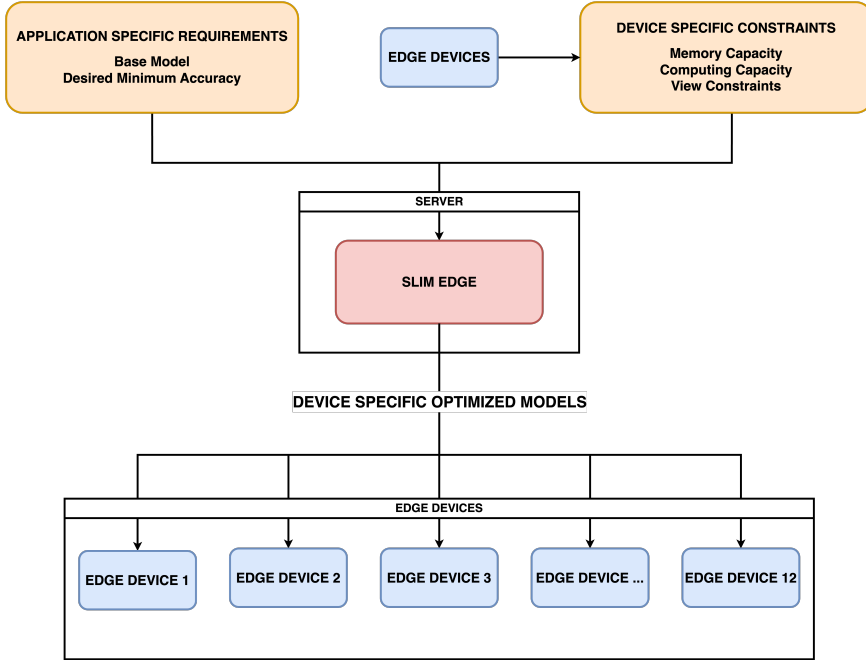


Figure 4: Top-Level Flowchart of SlimEdge

prises two distinct functional stages: a distributed feature extractor and a centralized aggregation stage.

Distributed Feature Extraction: This stage involves $V = 12$ independent convolutional subnetworks, $\phi_v(\theta_v)$, deployed across separate edge nodes. We utilize a modified VGG11 backbone, pre-trained on ImageNet1K and fine-tuned on ModelNet40. Each edge device v processes a local view x_v to produce a lower-dimensional feature embedding f_v : $f_v = \phi_v(x_v)$.

This decoupled design enables the SlimEdge to independently extract spatial information at each node, thereby facilitating parallel inference.

View Pooling and Classification: After extraction, the feature embeddings f_1, f_2, \dots, f_V are transmitted to the central server, while a view-pooling layer aggregates these inputs into a single global descriptor F using element-wise maximum-pooling: $F = \max_{v=1}^V (f_v)$.

This aggregation mechanism guarantees permutation invariance, making the model resilient to alterations in the sequence of camera inputs. Subsequently, the global descriptor F is subsequently passed to a central classifier, a fully connected network that predicts the final object class y .

3.3. *SlimEdge*

An overview of SlimEdge is shown in Figure 4. The application-specific requirements, i.e, the base model and the desired accuracy for the targeted application and the device specific constraints are sent to the server. The device constraints include the memory capacity and computing capacity of the device and the views captured by it. The server runs the optimization process evaluating the view-importance and considering the device and application specific constraints. The optimized model for each edge device is then created by the server and sent to the respective edge devices. In our experiments, we have selected distributed object recognition as the targeted application and have chosen the popular Multi-View Convolutional Neural Network (MVCNN) Su et al. (2015) architecture as the base model.

The MVCNN architecture comprises two stages: (i) a set of view-specific feature extractors, and (ii) a classifier that processes pooled features. The feature extractors are executed on the edge device, which communicates the data to the server as depicted in Figure 2. The server performs two tasks: running the optimization framework, SlimEdge, and pooling the features received from the edge devices. A detailed explanation of the SlimEdge is provided in the subsequent section.

3.4. *Components of SlimEdge*

SlimEdge, as depicted in Figure 4, is orchestrated by a central server. Unlike treating all views uniformly, the framework dynamically adjusts pruning intensity for each view based on its informational importance and the capabilities of the device. This approach effectively balances the global accuracy requirements with the resource constraints of individual devices.

3.4.1. *Model Pruning*

To address memory and latency constraints, filter-level pruning was applied to each view-specific feature extractor. This approach allowed SlimEdge to reduce the model’s size while maintaining its performance. Following Molchanov et al. (2017) Molchanov et al. (2017), the importance of the n -th filter was estimated using a first-order Taylor expansion of the loss function.

$$\mathcal{I}_j = \left| \sum_b \left(\frac{\partial \mathcal{L}}{\partial f_j^{(b)}} \right) f_j^{(b)} \right| \quad (1)$$

Where $f_j^{(b)}$ denotes the feature map produced by the filter on the b -th mini-batch, and \mathcal{L} is the classification loss as given in Equation 1. Filters with the lowest importance scores were iteratively removed, rather than in a single pass, to prevent

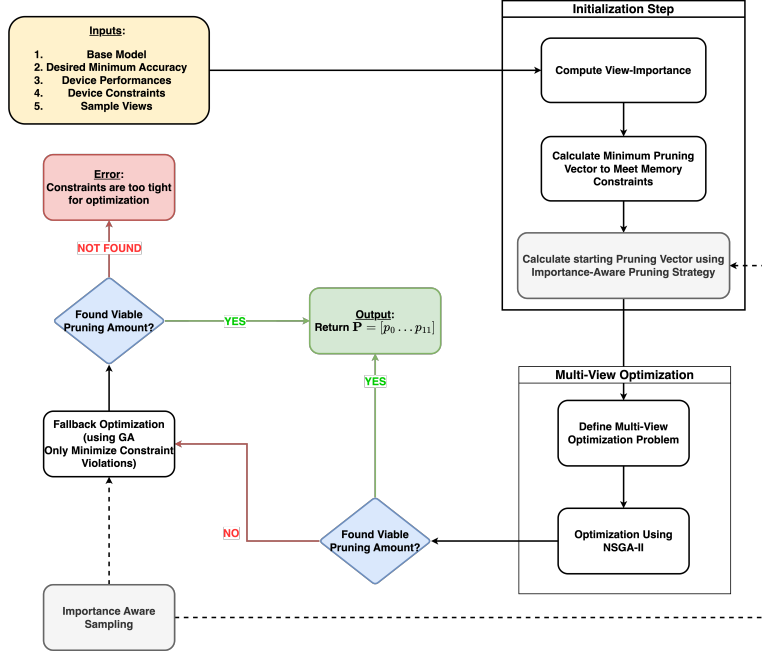


Figure 5: Component-Level Flowchart of SlimEdge

a sudden decline in representational capacity. The pruning schedule followed an exponential curve (Figure 5), with the pruning fraction at step i calculated as:

$$p_i = \frac{e^{-ki}}{\sum_{j=0}^T e^{-kj}} \cdot P \quad (2)$$

Where P is the total pruning fraction, k the decay rate, and T the number of steps (Equation 2). After each pruning step, the model was fine-tuned to regain lost accuracy. This approach is more efficient in preserving performance compared to one-shot compression Frankle and Carbin (2019).

3.4.2. Calculating the minimum pruning vector

To accelerate convergence, the minimum pruning required to satisfy per-device memory limits was computed through direct scaling. Given a target model size, the necessary pruning fraction p_v was determined by scaling the model size proportional to the ratio of the memory budget to the total model size (Equation 3). This yields a feasible lower bound on pruning for each view efficiently.

$$p_v = \max \left(0, 1 - \frac{S_{max,v}}{S_{original,v}} \right) \quad (3)$$

View	1	2	3	4	5	6	7	8	9	10	11	12
Importance (%)	7.2	10.5	7.9	7.7	7.8	8.6	9.1	8.7	8.6	7.6	8.3	7.9

Table 1: Importance of Each View

3.4.3. Computing view-importance

To quantify the contribution of individual views to classification accuracy, a large-scale ablation study was conducted. A discrete set of 51 pruning levels (ranging from 0% to 98%) was applied to each view, and the resulting models were fine-tuned and cached. For each test sample, feature tensors were precomputed and stored for all views and pruning levels. Subsequently, 55,665 random pruning configurations, each a 12-dimensional vector drawn from the discrete set, were evaluated by retrieving cached features, aggregating them via max-pooling (Eq. 4), and measuring mean class accuracy (Eq. 5). An XGBoost regressor Chen and Guestrin (2016) was used due to its lightweight nature and its ability to learn the data efficiently without overfitting. It was then trained to map pruning vectors to accuracy outcomes, and the resulting feature importance was interpreted as view salience scores. These scores, reported in Table 1, reveal non-uniform contributions across views, justifying asymmetric pruning.

$$F_{pooled}^{(s,P)} = \max_{v=1}^V (f_{s,v,p_v}) \quad (4)$$

$$A(P) = \frac{1}{C} \sum_{c=1}^C \frac{\text{correct}_c^P}{\text{total}_c} \quad (5)$$

3.4.4. Calculating device performance

Device capability was modeled as the inverse of inference time, normalized across the system. For a device v with measured inference time t_v , the performance metric was defined as in Equation 6.

$$d\text{Perf}_v = \frac{1/t_v}{\sum_{u=1}^V 1/t_u} \quad (6)$$

Where $d\text{Perf} \in [0, 1]^V$, ensuring that faster devices receive larger models during allocation.

3.4.5. Multi-Objective Formulation

Optimization was guided by a composite objective that balances accuracy, model size, and inference time. The total Fitness score for a pruning configura-

tion p was defined as a weighted sum:

$$R(p) = \alpha R_{acc} + \beta R_{size} + \gamma R_{time} + \delta R_{feas} \quad (7)$$

Equation 7, where each component is a smooth penalty or bonus.

1. R_{acc} penalizes deviations below a user-defined accuracy threshold via an exponential decay (Equation 8),
2. R_{size} rewards smaller models with a Gaussian-shaped Fitness score (Equation 9),
3. R_{time} similarly incentivizes lower latency (Equation 10),
4. R_{feas} provides an additional bonus when both accuracy and size constraints are satisfied (Equation 11).
5. The values of hyperparameters α, β, γ and δ are determined empirically as weights for the fitness score.

Fitness score for accuracy

The Fitness score for accuracy R_A can be calculated as an exponential function of the difference between the minimum acceptable accuracy and the accuracy of the configuration with a pruning configuration P . The difference between the accuracy of the pruned model configuration and the minimum accuracy is calculated as ΔA . Therefore, the Fitness score for accuracy, R_A , can be defined as in Equation 8.

$$R_A = \begin{cases} \left(e^{\frac{-\Delta A^{1.5}}{10\sigma_r^2}} \right), & 0 \leq \Delta A \leq 10^{-2}, \\ \left(e^{\frac{-\Delta A}{2\sigma_r^2}} \right), & \Delta A > 10^{-2}, \\ \left(e^{\frac{-|\Delta A|^{1.5}}{2\sigma_l^2}} \right), & \text{otherwise.} \end{cases} \quad (8)$$

Where σ_r represents the slope of the curve when the accuracy at the pruning configuration P is greater than the minimum accuracy A_{min} , and, σ_l represents the slope when $A(P) < A_{min}$. When $A(P) < A_{min}$, $\Delta A = 0$, therefore, when computing the reward, the absolute value of ΔA is calculated so that the exponent remains a real number.

Fitness score for model size

Similar to the Fitness score for accuracy, a Fitness score for model size is also computed. The maximum Fitness score is defined when the model size is 0 bytes, and the Fitness score gradually decreases as the model size increases. Defining the model size at the pruning amount p for view v as $S(p_v)$, and the maximum

model size defined by the user as $S_{max,v}$, for each view v , the difference in model size, ΔS can be calculated as $\Delta S = S(p_v) - S_{max}$. Therefore, the Fitness score for the size of the model can be computed as in Equation 9.

$$R_S = \begin{cases} \left(e^{\frac{-|\Delta S|^2}{10 \cdot \sigma^2}}\right) \cdot 100, & \Delta S > 10^{-2}, \\ 100, & -10^{-2} \leq \Delta S \leq 10^{-2}, \\ 100 + \frac{S_{max,v}}{S(p_v)}, & \text{otherwise.} \end{cases} \quad (9)$$

Here, σ is the slope of the curve, where higher σ values produce steeper slopes. The rewards thus can be plotted to a Gaussian curve, with the maximum value when the size of the model is 0.0 Bytes.

Fitness score for inference time

The Fitness score for inference time is maximum when the inference time is 0.0 seconds. As the inference time increases, the Fitness score decreases with a Gaussian slope. Therefore, the algorithm tries to minimize inference time, as a higher Fitness score is given for lower inference times. The Fitness score for inference time R_I can be calculated as in Equation 10:

$$R_I = \left(e^{\frac{-\max(T(P))^2}{2 \cdot \sigma^2}}\right) \cdot 100 \quad (10)$$

Where σ is the slope of the curve, where higher values of σ produce steeper slopes, and $T(P)$ is a list of the inference time of the model at each view v when $p_v\%$ of the model is pruned. The Fitness score is calculated for the maximum inference time taken by the MVCNN framework.

Fitness score for a more feasible model

If a model can be obtained with its accuracy greater than the minimum accuracy specified by the user, and its model size is less than the specified maximum model size, a Fitness score R_B is provided. The Fitness score for a more feasible model can be calculated as shown in Equation 11.

$$R_B = \left((A(P) - A_{min}) + \left(\frac{\sum_{v=1}^V S_{max,v} - S(p_v)}{V} \right) \right) \quad (11)$$

Here, $A(P)$ is the accuracy of the pruned models, A_{min} , $S_{max,v}$ the minimum accuracy specified by the user, and the maximum model size at each view v , respectively. $S(p_v)$ is the size of the model at view v when $p_v\%$ of it is pruned.

3.4.6. Importance-aware pruning strategy

The allocation of pruning intensity across views must reconcile two asymmetries inherent in distributed edge inference: (i) the unequal contribution of individual views to classification accuracy, and (ii) the heterogeneous computational capabilities of the devices hosting them. A uniform compression strategy ignores these factors, potentially sacrificing accuracy on high-salience views or failing to reduce latency on weaker devices. To address this, we formulate a principled allocation rule. We distribute "extra" pruning, beyond the mandatory minimum required for memory constraints, guided by a joint measure of view importance and device characteristics. Let V denote the total number of views (and corresponding edge devices). For each view $v \in 1, \dots, V$, let $P_{min,v}$ be the minimum pruning required to meet the strict per-device memory limit. We calculate a pruning weight λ for each device.

$$\lambda = \frac{(1 - I_v)(1 + dPerf_v)}{\sum_k [(1 - I_k)(1 + dPerf_k)]} \quad (12)$$

Here, I_v represents the view's importance score (where higher importance leads to a lower weight) and $dPerf_v$ represents the device's performance bottleneck (where higher inefficiency leads to a higher weight).

Next, we define a global extra pruning budget, P_{extra} , scaled by a factor λ relative to the total minimum pruning required across the system:

$$P_{extra} = \lambda \sum_{v=1}^V P_{min,v} \quad (13)$$

This global budget is then distributed back to individual devices based on their calculated weights (λ). The additional pruning amount for view v is defined as $\Delta P_v = \lambda \cdot P_{extra}$. Finally, the total pruning assignment for each view is the sum of its mandatory minimum and its allocated portion of the extra budget, capped at 99% to prevent total information loss:

$$P_{final,v} = \min(0.99, P_{min,v} + \Delta P_v) \quad (14)$$

This strategy ensures that weak devices or low-importance views absorb the majority of the compression, while critical features and capable devices are preserved.

3.4.7. Importance-aware sampling

To accelerate the convergence of the genetic algorithm in high-dimensional space, we employ an importance-aware sampling strategy. Instead of uniform

initialization, candidate pruning vectors are sampled from a Beta distribution parameterized by view salience scores I_v . Let v denote the number of views and N be the number of samples to be created, then the sampler constructs a matrix $X \in R^{N \times V}$ where each row $X_i \in [0, 1]^V$ corresponds to a pruning vector P for all views. The sampling is based on the Beta distribution parameterized for each view v using its importance score. We employ a beta distribution $B(\alpha, \beta)$ because its support is bounded in $[0, 1]$ naturally matching the normalized pruning ratios. The skewness toward 1.0 for low-importance views acts as a soft-constraint, guiding the genetic algorithm away from infeasible regions where high importance views are aggressively pruned. The beta distribution parameters are defined in Equation 18 as:

$$\alpha_v = (1 - I_v) \cdot \omega; \quad \beta_v = 1 \quad (15)$$

ω is defined to be a hyperparameter to scale the variance. The choice biases sampling so that views with low importance ($I_v \rightarrow 0$) yield higher values of α_v , push the distribution towards higher pruning amounts, while important features ($I_v \rightarrow 1$) maintain flatter distributions, allowing broader sampling. The first four rows of X are populated, with the first row, i.e, $X[0]$ storing the pruning amounts calculated by the distributed pruning framework. The second row, $X[1]$ stores the minimum pruning amounts that satisfy target model size constraints. $X[2]$ stores values as defined in equation 16, to favor more pruning on faster devices, while $X[3]$ acts as an aggressive variant of the distributed pruning framework, as equated in Equation 17.

$$X[2] = P_{min} \cdot \left(1 + 0.2 \cdot \frac{dPerf_v}{\sum dPerf} \right) \quad (16)$$

$$X[3] = \max(P_{min,v}, \text{Beta}(\alpha_v, \beta_v)) \quad (17)$$

The remaining rows are initialized as shown in Equation 18.

$$X_{i,v} = \max(p_{min,v}, \text{Beta}(\alpha_v, \beta_v)) \quad \forall v \in V \quad (18)$$

This initialization method speeds up convergence when the search space is high-dimensional, non-convex and expensive to evaluate.

3.4.8. Multi-objective problem

To analyze the trade-offs between inference speed, model accuracy, and model size, pruning is formulated as a constrained three-objective function. Let Equation 22 be the pruning amounts of V views, where P_{min} is the vector of minimum

pruning amounts computed.

$$X = [x_1, x_2, \dots, x_v]^T \in [P_{min}, 0.99]^V \quad (19)$$

The objective function is shown in Equation 20, and the decision variable X_v has been defined in Equation 21.

$$\text{minimize}_X [f_1(X), f_2(X), f_3(X)] \quad \text{s.t.} \quad g_1(X) \leq 0, \quad g_2(X) \leq 0 \quad (20)$$

$$X_v \in [P_{min,v} 0.99], \quad v \in V \quad (21)$$

The objective functions, inference time ratio, accuracy deviation penalty, and normalized Fitness score were formulated as shown in Equations 22, 23, and 24, respectively.

$$\mathbf{f}_1(X) = \frac{\max(T(X, dPerf))}{T_{baseline}} \quad \text{where} \quad T_{baseline} = \max_v (T_v(0, dPerf_v)) \quad (22)$$

$$\Delta_{acc} = A(X) - A_{min}, \quad \mathbf{f}_2(X) = \begin{cases} \kappa_g \cdot \Delta_{acc}; & \Delta_{acc} > 0 \\ \kappa_l \cdot |\Delta_{acc}|; & \Delta_{acc} \leq 0 \end{cases} \quad (23)$$

Where κ_g and κ_l are large weights when $\Delta_{acc} > 0$ and $\Delta_{acc} \leq 0$ respectively.

$$\mathbf{f}_3(X) = \frac{R(X)}{\max(R)} \quad (24)$$

Where $R(\cdot)$ is the objective function and $\max R$ is the maximum Fitness score possible. Two constraint functions were also initialized as in Equations 25 and 26.

$$\mathbf{g}_1(X) = A_{min} - A(X) \leq 0 \quad (25)$$

$$\mathbf{g}_2(X) = \max_v \frac{S_v(X_v)}{S_{max,v}} - 1 \leq 0 \quad (26)$$

Here, $S_v(X_v)$ is the size of the model at view v under pruning configuration X , with $S_{max,v}$ as its maximum allowable size. The Non-Dominated Sorting Genetic Algorithm-II (NSGA-II) Deb et al. (2002) was employed to minimize the objectives due to its superior performance in achieving the pareto-optimal front. NSGA-II works along with the importance-aware sampler, which evolves over 200 generations, optimizing the three objectives, with respect to the constraints, to provide a Pareto-optimal front that respects both accuracy and size requirements. The pruning vector with the least inference time is then selected as the best pruning amount.

3.4.9. Single-objective optimization

When Multi-Objective Optimization using NSGA-II fails to identify any feasible pruning configurations, a single-objective genetic algorithm (GA) Holland (1992) is employed that directly minimizes an aggregate penalty function. This fallback ensures that even in highly constrained regimes, the optimizer can produce a pruning vector that best approximates the constraints. The penalty function has been formulated as shown in Equation 27.

$$\mathbf{f}(\mathbf{x}) = \underbrace{\Phi \cdot \max(0, A_{\min} - A(x))}_{\text{accuracy violation}} + \underbrace{\sum_{v=1}^V \max(0, S_v(x_v) - S_{\max_v})}_{\text{size violation}} \quad (27)$$

Where $A(x)$ is the model accuracy under pruning x , A_{\min} the minimum required accuracy. $S_v(x_v)$ and S_{\max_v} the size of the view v under pruning x_v and its maximum allowed size. Φ is a large weighting constant to prioritize accuracy over size. GA then solves Equation 28:

$$x \in \min_{x \in [P_{\min}, 0.99]^V} f(x) \quad (28)$$

Where, V is the total number of views. This provides the best solution vector P that optimizes the model given the constraints. If the single-objective GA fails as well, the algorithm returns the minimum pruning amount P_{\min} required to meet the model size constraints.

4. Experimental setup

Extensive testing was conducted on various hardware configurations to validate the performance of the proposed algorithm. The varied hardware configurations have been detailed below:

4.1. Hardware platform

The experiments were executed across diverse CPU architectures to assess pruning effects under varying resource constraints.

1. Raspberry Pi Model A (Low-Tier)
2. Raspberry Pi 2 Model B (Mid-Tier)
3. Raspberry Pi 3 Model A+ (High-Tier)

The Thermal Design Power (TDP) ranged from 2W to 25W. This spectrum allowed consistent evaluation of model performance across heterogeneous computational environments.

4.2. Device simulation

1. Heterogeneous Devices: The computational power was sampled from a uniform distribution, inversely proportional to model inference latency. The memory capacities varied per device.
2. Homogeneous Devices: All devices had uniform computational power and identical memory allocations.

Each device was also assigned a view. For testing the algorithm, a random accuracy level was chosen, and random device performance metrics and memory capacity were used. Both accuracy and memory capacities were sampled from a beta distribution to account for any edge cases, i.e, very high model accuracy requirements but very low model size. Furthermore, the hardware devices mentioned were assigned various views to evaluate the performance of the algorithm in real-world scenarios with low-power, resource-constrained edge devices.

4.3. Model and dataset

A custom VGG11 model was employed, pre-trained on the ImageNet1K dataset (ref), which was then fine-tuned on the ModelNet40 dataset. This dataset includes 12 azimuthal viewpoints per object, each spaced 30 degrees apart, at a fixed elevation of 30 degrees. Furthermore, the final classification layer of the VGG11 architecture was modified from 1000 units to 40 output units to match the number of classes of the ModelNet40 dataset.

4.4. Evaluation metrics

SlimEdge was evaluated using three metrics:

1. Accuracy: Classification performance of each class after pruning.
2. Inference Time Reduction: Decrease in the inference time of the setup compared to the non-optimized setup.
3. Memory Violations: The number of instances where the model size exceeded the device memory constraints.

5. Results

The proposed algorithm was extensively tested to measure model performance on various configurations. The algorithm showed promising results, as it was able to optimize 980 of 1000 test cases run. Key experiments and their findings are presented below.

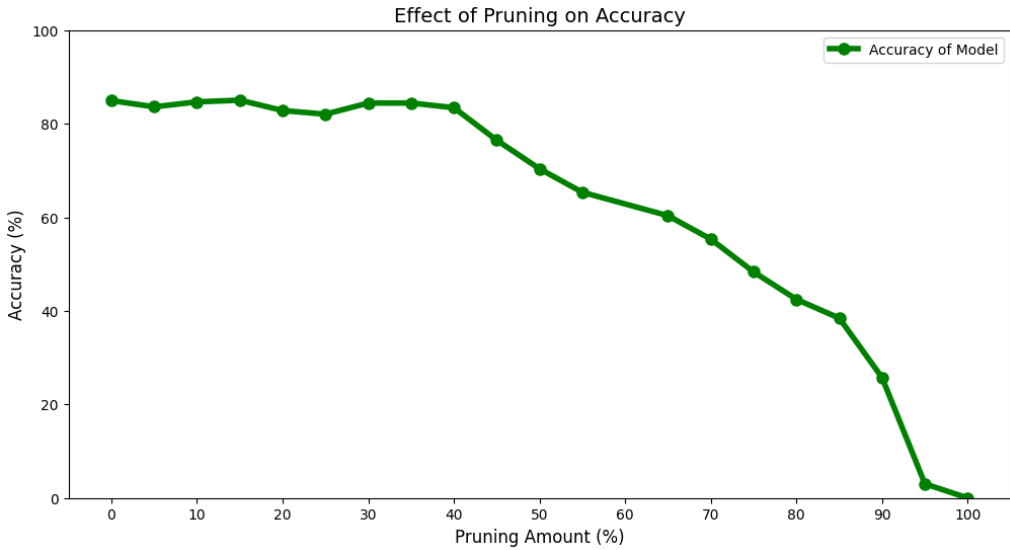


Figure 6: Effect of Filter Pruning on the Accuracy of the MVCNN Model

5.1. Impact of pruning on accuracy

All views of the MVCNN model were pruned uniformly using filter pruning and then fine-tuned on two epochs on subsets of the original dataset to compensate for the lost filters. The mean class accuracy results after pruning have been plotted below in Figure 6. The combined effect of Filter Pruning and fine-tuning allows the model to retain its accuracy, even at higher pruning amounts. As only the least essential filters are removed at each setup, the model can retain the filters that contribute the most to feature representation and decision boundaries, ensuring minimal degradation in performance, and fine-tuning after each pruning step further adapts the remaining parameters to compensate for the reduced performance, preserving accuracy.

5.2. Effect of pruning on inference time

On pruning all the views uniformly, a linear decrease in inference time was observed. The inference time was normalized using min-max normalization and has been plotted below in Figure 7. This enabled us to reduce the inference time of the MVCNN model significantly by pruning the model. The reduction in the number of filters after pruning reduces the number of computations required, thus speeding up inference.

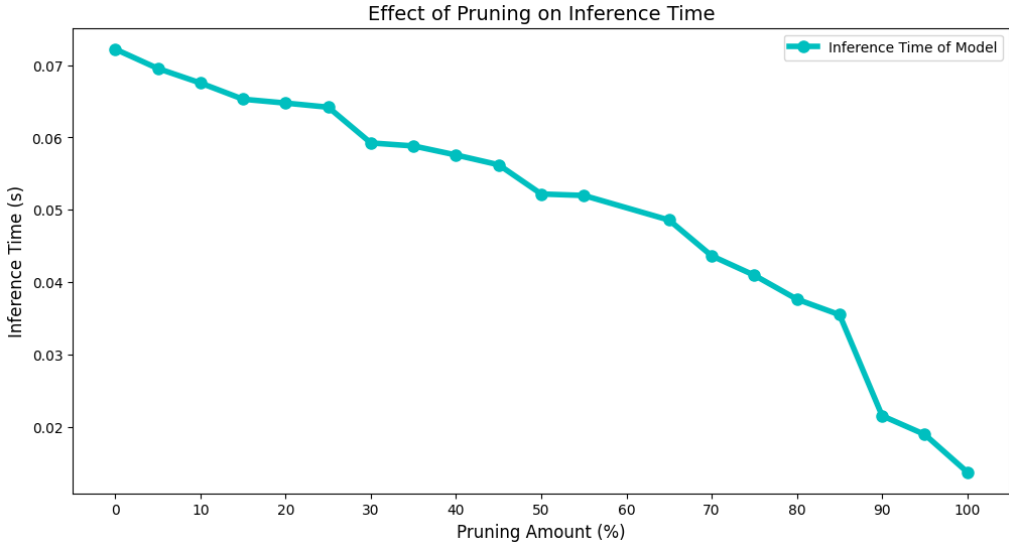


Figure 7: Effect of Pruning on Inference Time

5.3. Effect of pruning on model size

Similar to the effect of pruning on inference time, the model size also decreases with an increase in pruning. This is due to the number of filters being removed, with each element in each filter being 4 bytes in a float 32 model; the model size decreases linearly, as plotted below in Figure 8. As seen in Figure 8, the model size decreases linearly with an increase in pruning. This enables us to fit the pruned models in resource-constrained devices, effectively satisfying resource constraints.

5.4. Experiments

Experiments were conducted on the algorithm proposed to see its performance under various parameters and constraints. The framework showed robust performance in varied conditions, with each sub-part of the algorithm contributing in providing a model tailored for every situation. For every experiment, a modified VGG-11 model was used as the MVCNN model to train on the ModelNet40 dataset. This model had a mean class accuracy of 85% and a model size of 506.8 megabytes (MB).

5.4.1. Efficacy in heterogeneous environments

To validate the framework's ability to mitigate the "straggler problem" in mixed-tier clusters, we deployed the model across a diverse set of devices (Set-

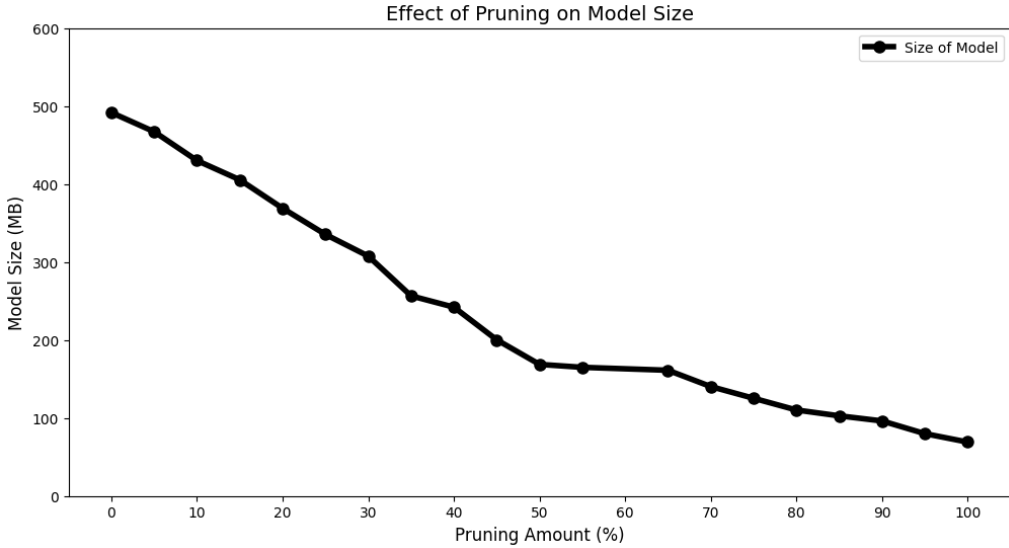


Figure 8: Effect of Pruning on Model Size

Device/View	1	2	3	4	5	6	7	8	9	10	11	12
Device Performance Factor	0.28	0.73	0.04	0.89	0.11	0.07	0.83	0.07	0.07	0.06	0.37	0.34
Device Memory Size MB	253.93	279.01	285.67	111.87	279.54	154.85	355.08	388.48	404.61	125.29	381.24	398.47

Table 2: Settings of Experiment 1

tings detailed in Table 2 and Table 3). In this configuration, views were assigned to devices with varying compute and memory profiles.

A minimum accuracy threshold of 83.10% was randomly chosen. Upon executing the algorithm, it provided the following results, graphed below in Figure 9. To evaluate the real-world reliability of this algorithm, a setup using 3 devices, namely, a Raspberry Pi Model A with 256 MB of RAM, a Raspberry Pi 2 Model B with 1 GB of RAM, and a Raspberry Pi 3 Model A+ with 512 MB of RAM, was created. The maximum size of the model is defined to be half the RAM of the device the model was deployed on. Therefore, the settings have been tabulated in Table 3. As seen in Figure 9 and Figure 10, SlimEdge successfully identified the computational bottlenecks. For instance, devices handling views 3, 5 and 9 (assigned to low-tier hardware) were automatically assigned aggressive pruning rates exceeding 90%. Conversely, the high-tier devices, such as View 2, retained larger model capacities. This device aware load balancing resulted in a 2.61x speedup compared to the uniform baseline.

Views 1 and 2 used a Raspberry Pi Model A, with 256 MB RAM and a 700MHz processor. Views 3, 6, 7, 8, 11, and 12 used a Raspberry Pi 3 Model

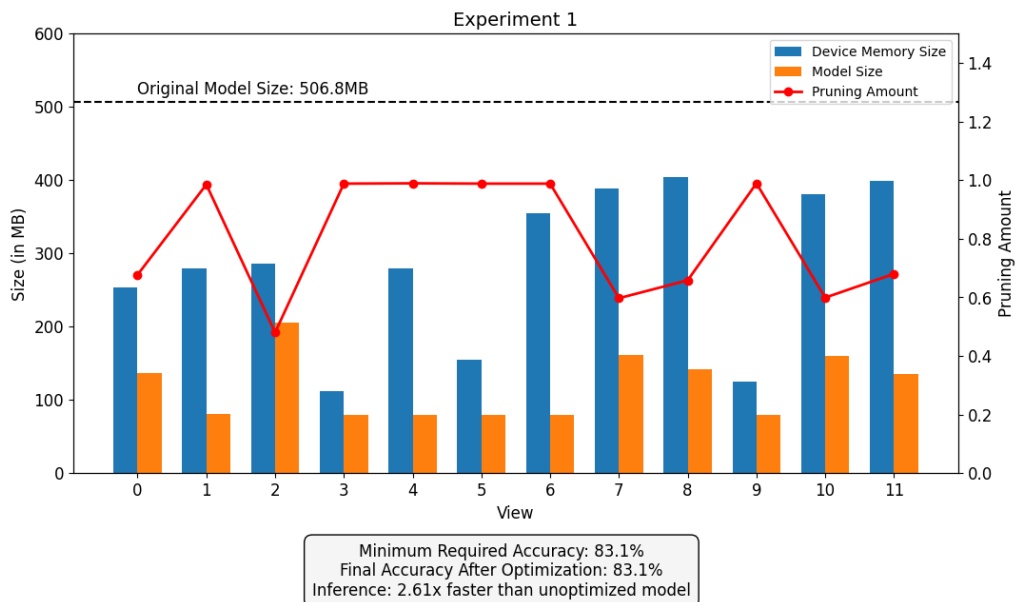


Figure 9: Results of Experiment 1

Device/View	1	2	3	4	5	6	7	8	9	10	11	12
Device Performance Factor	0.052	0.052	0.104	0.067	0.067	0.104	0.104	0.104	0.067	0.067	0.104	0.104
Max Model Size (MB)	128	128	256	512	512	256	256	256	512	512	256	256

Table 3: Settings of Experiment 2

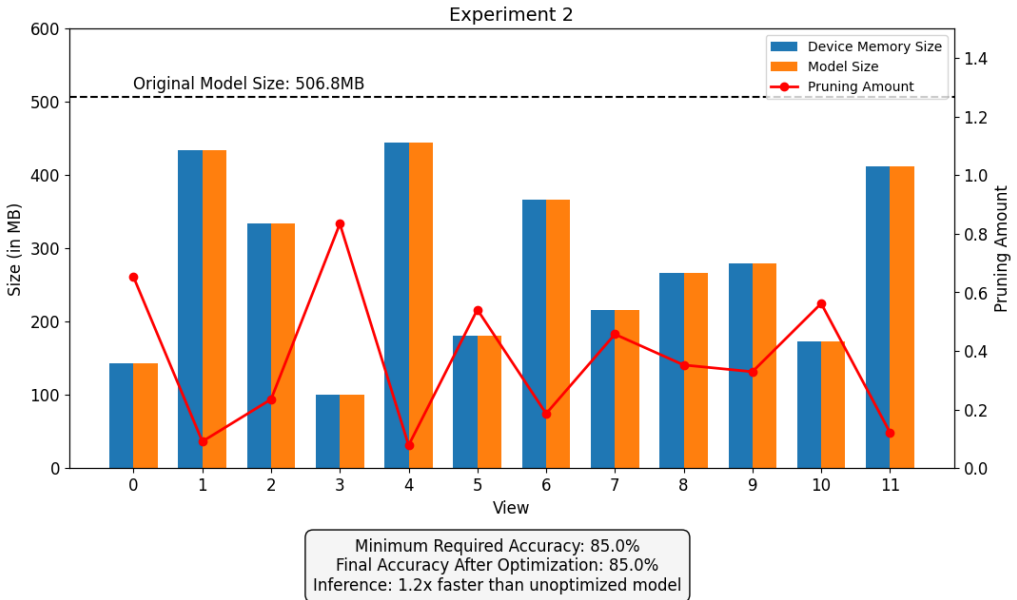


Figure 10: Results of Experiment 2

A+ with 512 MB of RAM and a 1400 MHz processor. The remaining views, 4, 5, 9, and 10, used a Raspberry Pi 2 Model B with 1 GB of RAM and a 900 MHz processor. The minimum required accuracy of the optimized MVCNN framework was defined to be 80.0%. The experiment was then conducted using these settings. The experiment results have been plotted below in Figure 10. Upon experimenting using the edge devices, a 3.94 times reduction in inference time was observed, while achieving an accuracy of 80.0%, which meets the minimum accuracy requirement. Furthermore, the algorithm was able to keep the optimized models within the device memory constraints. Experimenting with real-world edge devices was instrumental in evaluating the applicability of the algorithm. Pruning was concentrated on the devices with less memory and lower device performance scores so as to optimize inference time, while simultaneously meeting the accuracy constraints of the optimized MVCNN framework.

5.4.2. Performance under tight memory budgets

We further analyzed the framework's stability in regimes where feasible solutions are scarce due to tight accuracy and memory budgets, Table 4 and Table 5 detail these high-constraint scenarios, imposing an accuracy floor of 85% alongside server per-device memory caps.

Under these conditions, the solution space narrows significantly. As demon-

Device/View	1	2	3	4	5	6	7	8	9	10	11	12
Device Performance Factor	0.89	0.11	0.88	0.61	0.71	0.55	0.46	0.67	0.74	0.29	0.66	0.59
Max Model Size (MB)	143.6	434.5	334.5	100.5	444.6	181.2	366.1	215.5	266.4	279.2	173.4	411.4

Table 4: Settings for Experiment 3

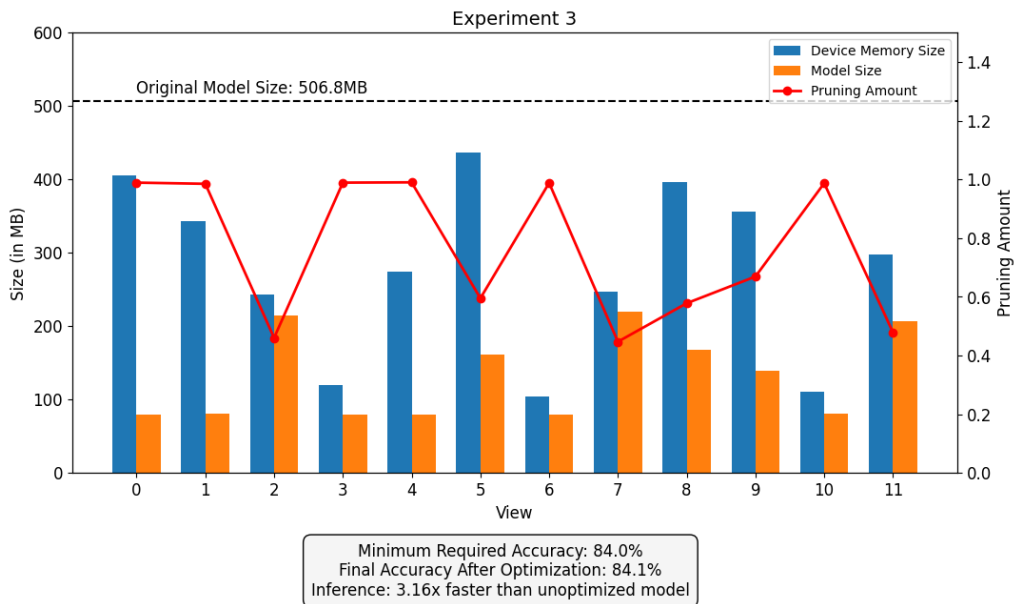


Figure 11: Results of Experiment 3

Device/View	1	2	3	4	5	6	7	8	9	10	11	12
Device Performance Factor	0.10	0.10	0.05	0.05	0.05	0.10	0.10	0.10	0.07	0.07	0.10	0.10
Max Model Size (MB)	256	256	128	128	128	256	256	256	512	512	256	256

Table 5: Settings of Experiment 4

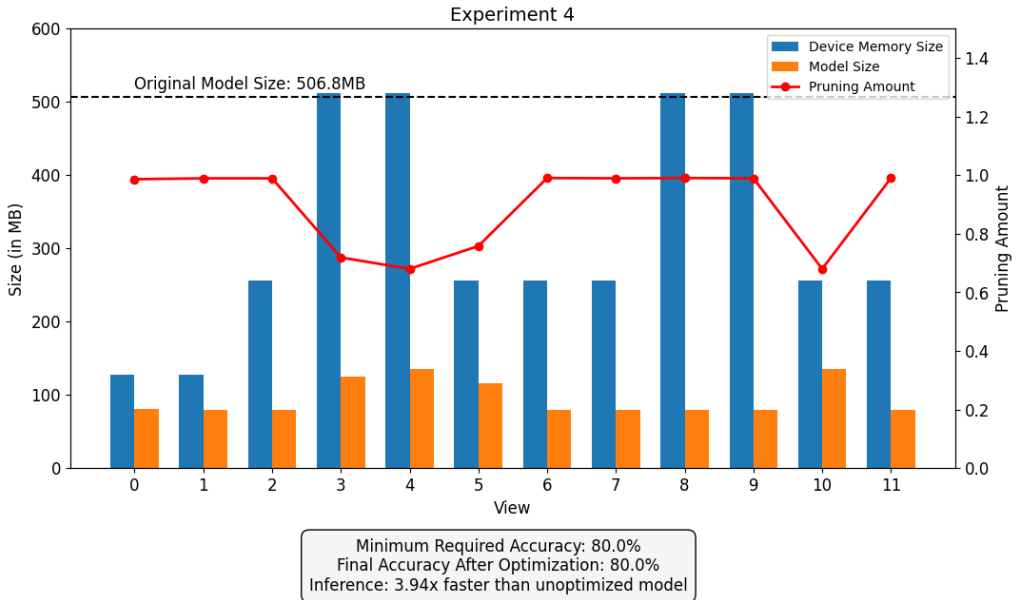


Figure 12: Results of Experiment 4

strated in Figure 11, the multi-objective search successfully converged to a configuration with zero constraint violations across all 12 devices. The fallback Single-Objective Genetic Algorithm proved critical in this regime; in fronts where the Pareto frontier initialization was infeasible, the Single Objective Genetic Algorithm fallback prioritized constraint satisfaction, ensuring a deployable model was found. This behavior was consistent in the extended analysis shown in Figure 12, where the framework maintained the 85.0% accuracy target despite the limited memory of the Low-Tier Raspberry Pi Model A devices (Views 3, 5 and 9). This confirms SlimEdge’s capability to sustain deployability even when hardware resources effectively saturate optimization constraints.

5.4.3. Bottleneck Alleviation Analysis

Finally, we isolated the impact of latency minimization by relaxing memory constraints while maintaining a high accuracy target of 84.0%. In the configuration detailed in Table 6, the optimizer was free to maximize model size on capable devices to recover accuracy, focusing pruning effects solely on reducing the inference time of the slowest node. The results in Figure 13 confirm that SlimEdge effectively decoupled pruning ratios from view importance when necessary. High-latency devices were pruned significantly deeper than low-latency counterparts, even for views with high informational salience. This targeted re-

Device/View	1	2	3	4	5	6	7	8	9	10	11	12
Device Performance Factor	0.02	0.03	0.33	0.81	0.49	0.21	0.18	0.46	0.08	0.71	0.86	0.48
Max Model Size (MB)	405.4	343.1	242.6	119.3	273.9	436.3	103.8	246.4	396.2	356.4	111.1	297.2

Table 6: Settings of Experiment 5

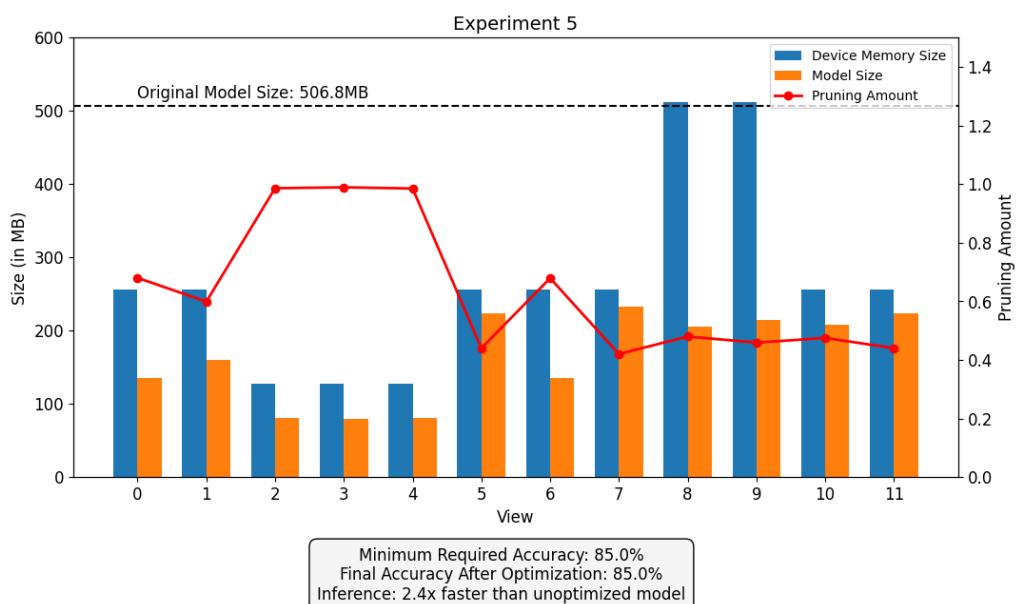


Figure 13: Results of Experiment 5

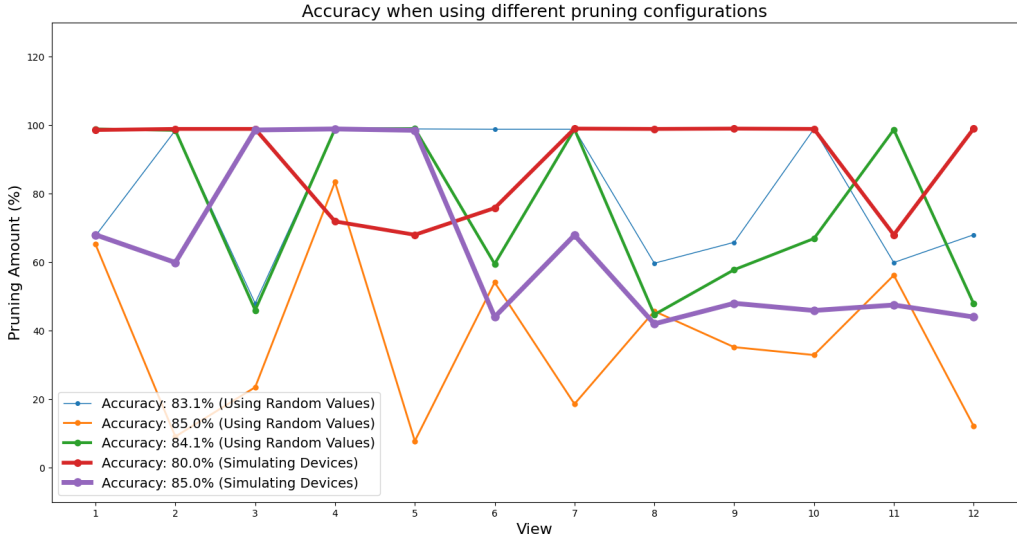


Figure 14: Accuracy of the MVCNN framework with various pruning configurations

duction of the critical path resulted in a 3.16x lower inference time compared to the non-optimized model. These findings indicate view-importance and device-capability must be optimized jointly to maximize distributed throughput.

SlimEdge has been able to optimize the MVCNN framework with highly constrained settings. The algorithm is able to maintain 85.0% accuracy while being 2.40 times faster than the original model. Furthermore, the algorithm was also able to optimize the models to fit within the device memory, thereby making the setup feasible for real-world deployment. The algorithm prunes models based on their contribution to the overall accuracy of the MVCNN framework, and the maximum model size that can be fit inside the memory of each device. This approach's ability to further prune models with high inference time on its edge device allows the algorithm to speed up the inference time by 2.40 times as well. Figure 14 presents the consolidated accuracy trends of the MVCNN framework across varying pruning levels. The results demonstrate a consistent pattern observed in all experimental setups: as the degree of pruning increases, the overall accuracy of the framework gradually decreases. This behavior reflects the inherent trade-off between reducing model size and computation versus maintaining classification performance, and it underscores the necessity of carefully selecting pruning levels to meet both accuracy and efficiency requirements in resource-constrained environments.

6. Conclusion

SlimEdge presents a framework for dynamic pruning techniques for distributed inference systems, tailored for both homogeneous and heterogeneous computational environments. Through rigorous experimentation, the effectiveness of the proposed approach in optimizing model performance while striking a balance between accuracy and efficiency by matching the required minimum accuracies of 83%, 84% and 85% with speedups of up to 3.94 times has been demonstrated. The integration of NSGA-II algorithms along with GA algorithms and the Objective Functions to optimize the model has yielded significant improvements in optimizing the MVCNN framework. Furthermore, the implications of such optimizations for edge devices have the potential to reshape the deployment of such models on resource-constrained devices. Across all experiments, the framework consistently identified feasible allocations that met accuracy and size requirements while predictably reducing distributed latency. When the minimum accuracy was set to 84.0%, the optimizer concentrated pruning on the devices that dominated the critical path and delivered a 3.16 times reduction in end-to-end inference time without violating the global constraint, which confirms that device-aware allocation together with importance-aware pruning can lower latency at a fixed quality target. The same behavior underpins the broader results, where pruning of low salience filters reduced FLOPs and parameters and therefore compressed both runtime and model size, while the importance values preserved capacity on views that contribute most to recognition, keeping the accuracy near the threshold. In heterogeneous settings, this produced speed-ups between 1.2 and 5.0 times while matching accuracy and respecting per-device memory ceilings, indicating practical deployability in resource-constrained multi-device environments. Methodologically, the design choices that shape the search were central to this outcome. The custom sampler biased candidates using view importance and the minimum viable pruning vector while seeding the population with informed configurations, which accelerated convergence in a high-dimensional and expensive space. The multi-objective formulation captured the coupled pressures of accuracy, size, and maximum device time, and the initialization for per-view minima provided strong starting points for admissible solutions. Under tighter regimes with high accuracy floors and small memory budgets, collapsing objectives into a single Fitness score acted as a reliable fallback that maintained solution quality and avoided constraint violations across devices. Together, these elements yield a route to distribute MVCNN-style models over constrained hardware while sustaining accuracy targets and meeting memory limits, and they motivate extensions that

integrate quantization, mixed precision, and communication-aware scheduling to further reduce energy and synchronization overheads at a larger scale.

References

Angrish, A., Bharadwaj, A., Starly, B., 2021. MVCNN++: Computer-Aided Design Model Shape Classification and Retrieval Using Multi-View Convolutional Neural Networks. *Journal of Computing and Information Science in Engineering* 21, 011001. URL: <https://asmedigitalcollection.asme.org/computingengineering/article/doi/10.1115/1.4047486>.

Baker, B., Gupta, O., Naik, N., Raskar, R., 2017. Designing Neural Network Architectures using Reinforcement Learning. URL: <http://arxiv.org/abs/1611.02167>, doi:10.48550/arXiv.1611.02167. arXiv:1611.02167 [cs].

Chen, L.C., Collins, M.D., Zhu, Y., Papandreou, G., Zoph, B., Schroff, F., Adam, H., Shlens, J., 2018. Searching for Efficient Multi-Scale Architectures for Dense Image Prediction. URL: <http://arxiv.org/abs/1809.04184>, doi:10.48550/arXiv.1809.04184. arXiv:1809.04184 [cs].

Chen, T., Guestrin, C., 2016. XGBoost: A Scalable Tree Boosting System, in: Proceedings of the 22nd ACM SIGKDD International Conference on Knowledge Discovery and Data Mining, pp. 785–794. URL: <http://arxiv.org/abs/1603.02754>, doi:10.1145/2939672.2939785. arXiv:1603.02754 [cs].

Deb, K., Pratap, A., Agarwal, S., Meyarivan, T., 2002. A fast and elitist multiobjective genetic algorithm: NSGA-II. *IEEE Transactions on Evolutionary Computation* 6, 182–197. URL: <https://ieeexplore.ieee.org/document/996017>, doi:10.1109/4235.996017.

Frankle, J., Carbin, M., 2019. The Lottery Ticket Hypothesis: Finding Sparse, Trainable Neural Networks. URL: <http://arxiv.org/abs/1803.03635>, doi:10.48550/arXiv.1803.03635. arXiv:1803.03635 [cs].

Holland, J.H., 1992. *Adaptation in Natural and Artificial Systems: An Introductory Analysis with Applications to Biology, Control and Artificial Intelligence*. MIT Press, Cambridge, MA, USA.

Liang, T., Glossner, J., Wang, L., Shi, S., Zhang, X., 2021. Pruning and quantization for deep neural network acceleration: A survey. *Neurocomputing* 461, 370–403. URL: <https://www.sciencedirect.com/science/article/pii/S0925231221010894>, doi:10.1016/j.neucom.2021.07.045.

Molchanov, P., Tyree, S., Karras, T., Aila, T., Kautz, J., 2017. Pruning Convolutional Neural Networks for Resource Efficient Inference. URL: <http://arxiv.org/abs/1611.06440>, doi:10.48550/arXiv.1611.06440. arXiv:1611.06440 [cs].

Su, H., Maji, S., Kalogerakis, E., Learned-Miller, E., 2015. Multi-view Convolutional Neural Networks for 3D Shape Recognition. URL: <http://arxiv.org/abs/1505.00880>, doi:10.48550/arXiv.1505.00880. arXiv:1505.00880 [cs].

Wu, Z., Song, S., Khosla, A., Yu, F., Zhang, L., Tang, X., Xiao, J., 2015. 3D ShapeNets: A Deep Representation for Volumetric Shapes. URL: <http://arxiv.org/abs/1406.5670>, doi:10.48550/arXiv.1406.5670. arXiv:1406.5670 [cs].

Yao, Y., Dong, B., Li, Y., Yang, W., Zhu, H., 2019. Efficient Implementation of Convolutional Neural Networks with End to End Integer-Only Dataflow, in: 2019 IEEE International Conference on Multimedia and Expo (ICME), pp. 1780–1785. URL: <https://ieeexplore.ieee.org/abstract/document/8784721>, doi:10.1109/ICME.2019.00306. iSSN: 1945-788X.

Yu, Q., Yang, C., Fan, H., Wei, H., 2020. Latent-MVCNN: 3D Shape Recognition Using Multiple Views from Pre-defined or Random Viewpoints. *Neural Process. Lett.* 52, 581–602. URL: <https://doi.org/10.1007/s11063-020-10268-x>, doi:10.1007/s11063-020-10268-x.

Zhao, Z., Barjough, K.M., Gerstlauer, A., 2018. DeepThings: Distributed Adaptive Deep Learning Inference on Resource-Constrained IoT Edge Clusters. *IEEE Transactions on Computer-Aided Design of Integrated Circuits and Systems* 37, 2348–2359. URL: <https://ieeexplore.ieee.org/document/8493499>, doi:10.1109/TCAD.2018.2858384.